3D.2

Choosing a Boundary-Layer Parameterisation for Tropical Cyclone Modelling

Jeffrey D. Kepert *

Centre for Australian Weather and Climate Research

Extended abstract, AMS 30th Conference on Hurricanes and Tropical Meteorology

Note: This extended abstract is closely based on Kepert (2012)

ABSTRACT

The boundary layer in a tropical cyclone is in some respects unlike that elsewhere in the atmosphere. It is therefore necessary to evaluate boundary-layer parameterisations for their suitability for use in tropical cyclone simulation. Previous work has shown substantial sensitivity to the choice of scheme and identified specific shortcomings in some schemes, but without recommending which schemes are most suitable. Here, several schemes, representative of those available in popular modelling systems, are reviewed and applied in a simplified modelling framework. Based on a comparison with observations and on theoretical grounds, one popular class of schemes is shown to be badly flawed in that it incorrectly predicts the near-surface wind profile, and therefore should not be used. Another is shown to be sensitive to diagnosis of the boundary-layer depth, a difficult problem in the core of the tropical cyclone, and caution is advised. The Louis boundary-layer scheme and a higher-order closure scheme are, so far as we can discern, without major problems, and are recommended. The recommendations and discussion herein should help users make a more informed choice of boundary-layer parameterisation, and to better understand the results that they obtain.

1. Introduction

The boundary layer is an important part of tropical cyclones, since boundary-layer processes regulate the sources of heat and moisture, and sink of momentum, that help determine the storm intensity, and because it is through the boundary layer that much of the impact on humat from much of the atmospheric boundary layer because of the strong effect of the cyclone's rotation upon its dynamics (Rosenthal 1962; Eliassen 1971; Eliassen and Lystad 1977; Kepert 2001; Kepert and Wang 2001).

The impact of the surface fluxes on intensity substantially motivated for the recent effort into better parameterising these fluxes under extreme wind conditions, through both measurement (Powell et al. 2003; Black et al. 2007; French et al. 2007; Zhang et al. 2008a; Drennan et al. 2007) and theory (Andreas 2004; Donelan et al. 2004; Makin 2005; Bye and Jenkins 2006; Moon et al. 2007). The main result of this effort has been that the drag coefficient does not increase indefinitely with wind speed, but is capped or possibly begins to decrease above wind speeds of about 30 m s^{-1}, while the moisture transfer coefficient is constant up to at least 33 m s^{-1}.

In contrast, less effort has been devoted to the more difficult problem of determining the turbulent fluxes of enthalpy and momentum *above* the surface layer. Gall et al. (1998), Katsaros et al. (2002), Foster (2005), Lorsolo et al. (2008) and Zhang et al. (2008b) have shown the presence of roll-like features and noted that these may be significant in determining the fluxes. Moss (1978) and Moss and Merceret (1976) presented turbulence measurements in the periphery of Hurricane Eloise, while Zhang et al. (2009) presented aircraft measurements of the turbulent fluxes between outer rainbands and deduced the turbulence kinetic energy (TKE) budget. Zhang et al. (2011a) estimated the stress, TKE and eddy diffusivity near the top of the inflow layer in the inner core of Hurricane Hugo. Lorsolo et al. (2010) extensively mapped the TKE in several storms using Doppler radar measurements. Nevertheless, there is presently insufficient data to directly validate turbulent flux parameterisations above the surface layer in tropical cyclones.

Several modelling studies have demonstrated that the storm intensity and structure are sensitive to the parameterisation of these fluxes. Braun and Tao (2000) compared four schemes (two local, one

* *Corresponding author address:* Jeffrey D. Kepert, Centre for Australian Weather and Climate Research, GPO Box 1289K, Melbourne 3001. Australia.
E-mail: J.Kepert@bom.gov.au

higher-order and one nonlocal closure[1]) in MM5 simulations of Hurricane Bob, and found differences of up to $15\,\mathrm{m\,s^{-1}}$ in intensity and 16 hPa in central pressure, as well as substantial differences in the rainfall. These differences were reduced but not eliminated when all schemes were modified to use the same parameterisation of the surface fluxes, although the Medium-Range Forecast (MRF) scheme remained an outlier. Smith and Thomsen (2010) compared several schemes, including examples of local, nonlocal and higher-order closures, in an idealised f-plane setting and using the same surface-flux parameterisation, and found significant variation in storm structure, intensity, and rate of intensification. While they noted deficiencies in some schemes, they were unable to recommend any one as "optimum". Nolan et al. (2009a,b) compared a local and a higher-order scheme, presenting a more detailed analysis of the boundary-layer structure than the other studies. While there were some differences between the schemes, they generally reproduced the observed structure of the tropical cyclone boundary layer "remarkably well".

Two studies have compared parameterisations in a more idealised setting, in which the boundary layer flow is diagnosed as the response to a prescribed pressure field. Foster (2009) considered three different prescribed vertical structures of the turbulent diffusivity with various magnitudes and vertical scales, and found substantial variation. In contrast, Kepert (2010a,b) briefly compared a higher-order closure with a simple nonlocal closure, and found that they produced similar results in the cyclone inner core, but markedly different results at radii where there was subsidence, since only the higher-order closure was sensitive to the resulting increase in static stability.

The large spread in simulated tropical cyclone behaviour in the full-physics modelling studies discussed above suggests two possibilities. Perhaps the cyclone is very sensitive to small changes in the boundary layer, such that minor differences between parameterisations lead to large differences in the simulations. This situation might plausibly arise either directly, or through a nonlinear feedback in which the boundary layer and the atmosphere above are each dependent on the other. Certainly this latter feedback exists; the question is whether the feedback between the boundary layer and the rest of the vortex is strong enough to explain the sensitivity to parameterisation. Another possibility is that there may be large differences between the boundary layer parameterisations, sufficient to explain the differences in these simulations.

The possibility of large differences between the parameterisations is of concern. These parameterisations all aim to do the same thing—represent the effect of the turbulent fluxes—albeit by quite different methods. Large differences would imply either insufficient scientific knowledge, or that some schemes contain errors. This paper demonstrates that there are large differences between simulations with schemes that are commonly used for TC simulation, and examines the reasons for these differences.

The main tool used is the diagnostic tropical cyclone boundary layer model of Kepert and Wang (2001, henceforth KW01), which diagnoses the boundary layer flow in response to a prescribed pressure field representative of the rest of the cyclone. With the pressure field prescribed, the influence of the boundary layer on the rest of the cyclone is removed, restricting attention to the direct effect of differences in the parameterisations. A number of boundary-layer parameterisations, including those used in the above modelling studies, have been analysed and a representative set implemented in the model. All experiments use the same parameterisations of the surface fluxes, removing another source of variation. It is shown that one widely-used class of PBL parameterisations has serious deficiencies, including a severe inability to reproduce observations, and should not be used. A further class is shown to produce poor simulations in certain circumstances. The reasons are discussed, and appropriate caution in using such schemes is recommended. The discussion of these model results is supported, where appropriate, by theoretical considerations of the turbulence structure.

Models such as MM5 and WRF offer the user a choice from several boundary-layer schemes. It is hoped that the analysis herein will help users avoid certain parameterisations that are unsuitable for tropical cyclone simulation, and to make a better-informed choice from the remainder. The analysis may also help users to diagnose, understand and perhaps rectify poor behaviour should it occur with other schemes.

A brief introduction to boundary-layer parameterisation is given in section 2, to provide non-experts with sufficient background to understand the main issues. This is followed by a survey of parameterisation methods and the presentation of those used here. Section 4 describes the model, and section 5 presents simulations with each parameterisation. These results are discussed in section 6, followed by the conclusions.

[1] Types of turbulence closure are discussed in section 3.

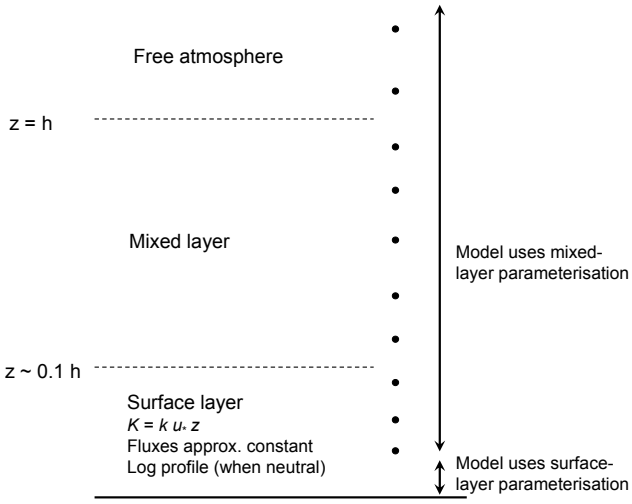

FIG. 1. Schematic illustration of the relationship between the parts of the atmospheric boundary layer and a numerical model. The left part of the figure shows the atmospheric surface and mixed layers, while the right part indicates the model, with the dots showing the model levels and the arrows showing which parameterisation is typically used for the fluxes between the levels. The depths of the surface and mixed layers, and hence the number of model levels that fall within each, will vary with the meteorological situation. As the model typically uses its mixed-layer parameterisation for all except the lowest layer, this parameterisation must be capable of modelling surface-layer behaviour when appropriate.

2. Components of a typical boundary-layer parameterisation

The planetary boundary layer is customarily divided into the surface or constant-flux layer, and the mixed layer, as shown schematically in Fig. 1. There is in reality no distinct division between these layers, but the surface layer is typically taken as that in which the fluxes vary by less than 10% from their surface value, and to occupy about the lowest tenth of the boundary layer.

a. Surface-layer parameterisation

Under neutral conditions[2], the vertical profiles of momentum, heat and moisture in the surface layer are observed to be logarithmic in height.

Prandtl (1932) suggested that the vertical turbulent flux of a quantity α near a flat surface can be parameterised by a flux-gradient relationship

$$\langle w'\alpha' \rangle = K \frac{\partial \alpha}{\partial z}, \tag{1}$$

where the turbulent diffusivity is proportional to distance from the surface,

$$K = k u_* z. \tag{2}$$

Here, k is von Kärmän's constant and u_* is the friction velocity, defined by

$$\tau = \rho u_*^2 \tag{3}$$

where τ is the momentum flux magnitude at the surface. Consider the wind component u in the direction of the surface flow, and flow in the surface layer, so that the flux can be assumed to be nearly constant with height. Then the momentum equation for steady, horizontally homogeneous flow neglecting vertical advection (since $w = 0$ at the surface) and rotation[3] reduces to

$$\frac{\partial u}{\partial z} = \frac{u_*}{kz} \tag{4}$$

which when solved gives the logarithmic profile,

$$u = \frac{u_*}{k} \log\left(\frac{z}{z_0}\right). \tag{5}$$

Here z_0 is the integration constant, known as the roughness length. These equations, and similar ones for heat and moisture, comprise one standard method for parameterising the near-surface fluxes. An alternative is via the bulk formulae. For momentum, given a drag coefficient C_D and wind speed at the lowest model level u_1,

$$\tau = \rho C_D u_1^2, \tag{6}$$

so the approaches are related through

$$C_D = \left(\frac{k}{\log(z_1/z_0)}\right)^2 \tag{7}$$

where z_1 is the height of the lowest model level; note that C_D therefore depends on the reference height. In the atmosphere, these formulae need to be modified to account for the effects of stability, often by using Monin-Obukhov similarity theory. Both forms are widely used in atmospheric modelling for parameterising the fluxes between the surface and the lowest model level.

[2]Here, as is customary in boundary-layer meteorology, "neutral" means that the turbulence is predominantly produced by shear, with buoyant production/destruction of TKE being relatively small; that is, the Richardson number Ri ≈ 0.

[3]In the tropical cyclone *surface* layer, $\tau \sim 1\,\mathrm{N\ m^{-2}}$ and the rotation and advection terms can be neglected.

b. Mixed-layer parameterisation

Above the surface layer, flux-gradient relationships (1) are widely used, but the diffusivity does not increase indefinitely with height as in (2). However, it is highly desirable that the turbulence parameterisation in this region blends smoothly with that in the surface layer. Firstly, the atmosphere does not contain a distinct division between the two layers. Secondly, the depth of the surface layer depends on the meteorological situation so, referring to Fig. 1, the number of model levels that fall within the surface layer will vary. Atmospheric models typically use their surface-layer parameterisation only for the fluxes between the earth's surface and the model's lowest level, so the mixed-layer parameterisation must be capable of modelling surface-layer behaviour when the atmospheric surface layer extends above the lowest model level. This requirement also reduces the sensitivity of the simulations to the precise configuration of the model's vertical levels, and ensures that the solution will converge as the vertical resolution increases. Indeed, the surface-layer is better understood and more easily measured than the mixed layer, so mixed-layer parameterisations are often tested on their ability to reproduce surface-layer measurements.

Turbulence parameterisations frequently contain a length scale l, which represents the scale of the energy-containing eddies. Near the surface, the proximity of the surface constrains the size of these eddies, an idea that leads to Prandtl's surface-layer parameterisation (2), in which the length scale (or mixing length) is $l = kz$. This length scale does not increase indefinitely with height, and Blackadar (1962) suggested a form which has since become widely, although not universally, used,

$$l^{-1} = (kz)^{-1} + l_\infty^{-1} \tag{8}$$

where l_∞ is the asymptotic mixing length. For small z, (8) gives $l \approx kz$, while $l \to l_\infty$ as $z \to \infty$. This form is most appropriate for neutral and unstable conditions; in statically stable conditions the stratification acts to limit the vertical extent of the turbulent eddies and l may be modified accordingly. This paper will use the value from KW01, $l_\infty = 80\,\mathrm{m}$, whenever (8) is used; the sensitivity to other choices is discussed in section 5b.

The above brief introduction applies to a near-neutral boundary layer, appropriate for the tropical cyclone case, where shear is the dominant source of turbulence (Zhang et al. 2009). Strong thermal effects can significantly change matters. These effects include:

i. With strong surface heating, buoyant eddies can mix through the stable stratification in the upper boundary layer, transferring heat upwards against the mean potential temperature gradient. This phenomenon is called the countergradient heat flux; it may be parameterised by modifying the flux-gradient relationship.

ii. Stable stratification can limit the vertical extent of turbulent eddies, and hence the mixing length. It also destroys TKE.

iii. If the turbulence is predominantly generated by buoyancy and the shear-generation is negligible, then a condition known as free convection arises (this term does *not* refer to clouds).

However, these situations depend on strong thermal effects and, while crucial to obtaining good simulations in, say, diurnally-varying boundary layers over land, might reasonably be expected to be less important in the tropical cyclone core where the buoyancy effects on the turbulence are weaker (Zhang et al. 2009). Evidence will be presented in section 5 to support this expectation.

3. Boundary-layer parameterisations used in tropical cyclone simulation

This section introduces some common boundary-layer parameterisation methods, and discusses the implementation of a representative of each into KW01's model. The schemes considered are summarised in Table 1. These implementations do not use the actual code used in other models, since those models use different numerics to KW01. Rather, the equations to calculate K were implemented in the KW01 model and its numerical solution used. In all cases, the surface fluxes are calculated by bulk formulae, with the drag coefficient given by

$$C_D = \min(0.7 + 0.065u_{10}, 2) \times 10^{-3}, \tag{9}$$

(Smith and Montgomery 2008) where u_{10} is the 10-m wind speed in m s^{-1}, and the heat transfer coefficient $C_h = 0.0011$. This surface flux parameterisation is consistent with recent high wind-speed measurements (Powell et al. 2003; French et al. 2007; Black et al. 2007) and was used by Kepert (2010a,b).

A survey of which boundary layer parameterisations are used in the recent tropical cyclone literature is presented in the final subsection.

TABLE 1. Summary of the formulation of the turbulent diffusivity in the four parameterisations considered.

Parameterisation	K	l	Remarks
Bulk/Hi-Res	$l^2 S f(\mathrm{Ri})$	40 m	$f(\mathrm{Ri}) = \max(1 - \mathrm{Ri}/\mathrm{Ri}_c, 0)$
Louis	$l^2 S f(\mathrm{Ri})$	Eq. 8	Uses version VI $f(\mathrm{Ri})$
Neutral Louis	$l^2 S$	Eq. 8	
Nonlocal KPP	$k u_* z (1 - z/h)^p$	—	p and h are prescribed
Mellor-Yamada	$l q S_M$	Eq. 8	
Neutral Mellor-Yamada	$0.39 l q$	Eq. 8	$S_M = 0.39$ in neutral conditions

a. The Bulk and High-Resolution schemes of MM5.

These schemes parameterise the diffusivity by

$$K = l^2 S f(\mathrm{Ri}) \tag{10}$$

where l is constant, S is the magnitude of the vertical wind-shear, and $f(\mathrm{Ri}) = \max(1 - \mathrm{Ri}/\mathrm{Ri}_c, 0)$ for a critical Richardson number $\mathrm{Ri}_c = 0.25$. This scheme is known as a first-order local closure; "first-order" since there are no prognostic equations for turbulence quantities, and "local" since the diffusivity at any point depends only on conditions at that point.

The Bulk scheme originated in a paper on the nocturnal boundary-layer by Blackadar (1976), which argued for (10) based on a simplified turbulence model. A constant mixing length of $l = 28$ m was used, later increased to 40 m (Blackadar 1979), reasonable for this highly stratified situation. The violation of the expected near-surface behaviour ($l \approx kz$) can perhaps be justified given of the coarse vertical resolution of that period and the effect of stability on the mixing length. Indeed, Blackadar (1976) notes immediately after presenting (10) that a form of l which is tangent to $l = kz$ at the surface would be preferred if the stratification was less stable.

The "High-Resolution" (henceforth Hi-Res) scheme is described by Zhang and Anthes (1982), and appears to owe its name to the title of that paper. It considers four stability classes for the surface flux parameterisation, the details of which are unimportant here, and two stability classes for the mixed-layer fluxes: free convection and otherwise. Except under free convection conditions , the mixed-layer fluxes are as in the bulk scheme, except that the mixing length is written as kl rather than l and increased to $kl = 40$ m, the value used here. When free convection occurs, mixing occurs simultaneously through the whole of the mixed layer, with the intensity of the mixing determined by the thermal structure of the mixed layer and the intensity of the surface heat flux. However, this module is triggered only for strong surface heating and weak vertical wind shear, conditions that do not occur in tropical cyclones.

Unfortunately, Blackadar's caution about the need for a more appropriate near-surface form of l in conditions that are not highly stratified was not implemented in either scheme[4]. Thus, while many refer to the latter parameterisation as the "Blackadar", we prefer "Hi-Res" as his prescription was not followed.

Observations show that the wind shear in the tropical cyclone boundary layer increases towards the surface in the tropical cyclone boundary layer (Franklin et al. 2003; Kepert 2006a,b). The Bulk and Hi-Res parameterisations will thus give maximum diffusivity at or near the lowest model level, a structure that is apparent in Braun and Tao (2000, Fig. 15) and Smith and Thomsen (2010, Fig. 8).

In a neutral near-surface constant-flux layer with (10) and l constant, similar arguments to those in section 2 lead to

$$\frac{\tau}{\rho} = K \frac{\partial u}{\partial z} = l^2 \left(\frac{\partial u}{\partial z} \right)^2 \tag{11}$$

or

$$\frac{\partial u}{\partial z} = \frac{1}{l} \sqrt{\frac{\tau}{\rho}}; \tag{12}$$

that is, the wind speed varies nearly linearly with height. Hence, in near-neutral conditions, the Bulk and Hi-Res parameterisations will not match smoothly with a logarithmic surface layer and will produce incorrect results when the atmospheric surface layer extends above the lowest model level. Further, the modelled profiles (including the near-surface logarithmic layer implicit in the surface-layer parameterisation) will depend on the height of the lowest level in the model; changing the vertical resolution will change the simulation. We hypothesise that this matter contributed to the large sensitivity to vertical resolution that Kimball and Dougherty (2006) found in their experiments, which used the Hi-Res scheme and varied the height of the lowest model level.

Consistency with the logarithmic surface layer can be restored by making $l \approx kz$ near the surface. That modification leads to our next parameterisation.

[4]This omission was confirmed by examining the code (subroutines blkpbl and hirpbl in MM5 version 3 release 3-7).

b. The Louis PBL scheme

The Louis scheme, originally developed for the ECMWF operational model (Louis 1979) and subsequently refined (Louis et al. 1982), has been widely used in operational NWP. The diffusivity is parameterised by (10), so the Louis scheme is another local closure. However, it differs from the Bulk and Hi-Res schemes in three significant ways: (i) the Blackadar mixing length (8) is used instead of a constant, (ii) the diffusivities for heat and momentum differ, and (iii) the stability functions were more extensively verified and are more complex. Here, version VI of the stability functions is used[5]. Our scheme differs from Louis et al. (1982) in one way; we use $l_\infty = 80\,\mathrm{m}$ as in the higher-order closure scheme, instead of $l_\infty = 150\,\mathrm{m}$[6]. This change reduces the mixing in the middle to upper boundary layer; the sensitivity of the solutions to l_∞ is discussed in section 5b. We implement also a neutral version of the Louis scheme, that is, with $f(\mathrm{Ri}) = 1$.

The use of Blackadar's length scale would be expected from the preceding discussion to lead to better modelling of the flow near the surface; section 5b shows that this expectation is correct.

c. Nonlocal closures

The preceding two schemes are known as local closures, since the diffusivity at each level depends only upon conditions at that level. This dependence is nonlinear and can be highly sensitivity to those conditions, so implementation needs care to avoid numerical instabilities (Kalnay and Kanamitsu 1988). A further consideration is that the turbulence may be reasonably regarded as being driven from the surface up to the entrainment layer at the top of the boundary layer, and so perhaps the diffusivity could be formulated to be insensitive to the intervening levels.

Nonlocal closures take several forms. Those of the KPP (K-profile parameterisation) type explicitly diagnose the boundary layer top h, and fit a parametric profile of K to h and the surface conditions. The usual form of K was first introduced by O'Brien (1970),

$$K = ku_* z(1 - z/h)^p \tag{13}$$

with the shape parameter $p = 2$. This formula is essentially empirical; with $p = 2$ it is the lowest-degree polynomial that matches the expected conditions at the top and bottom of the boundary layer. It is tangent to the surface-layer's $K = ku_*z$ at the surface, has a maximum of

$$K_{\max} = ku_* h\,\frac{p^p}{(p+1)^{p+1}} \tag{14}$$

at $z = h/(p+1)$, and returns smoothly to $K = 0$ at $z = h$. The mean to height h is

$$\overline{K} = \frac{ku_* h}{(p+1)(p+2)}. \tag{15}$$

Note that both $K_{\max}$ and $\overline{K}$ are proportional to h.

The MRF scheme (Hong and Pan 1996) in MM5 and WRF is a development of a KPP scheme by Troen and Mahrt (1986), and includes parameterisations for the counter-gradient heat flux and the effects of stability. Further refinement (Noh et al. 2003; Hong et al. 2006) has resulted in the YSU scheme available in WRF. The Unified Model of the UK MetOffice uses a sophisticated version of a KPP scheme in unstable conditions, in which the parameterised profiles can also represent turbulence initiated away from the surface, such as due to cloud-top cooling in a stratocumulus deck (Lock et al. 2000). A local closure is used in stable conditions.

K-profile closures only represent the mixing within the boundary layer, but in reality, weaker turbulence and vertical mixing is present throughout the atmosphere. A separate parameterisation to represent mixing above h is therefore needed; the MRF and YSU schemes use a Louis scheme for this purpose.

Determining h is an important consideration in formulating KPP closures, and one of the main differences between the schemes mentioned above. Because the bulk Richardson number criterion used for h in MRF produced excessively strong mixing in shear-dominated situations (Noh et al. 2003), it was replaced by a condition using the potential temperature profile in the YSU scheme (Hong et al. 2006).

The definition of h is important, since it determines not only the vertical extent of the mixing, but also the peak and mean magnitudes of K. Zhang et al. (2011b) analysed the boundary-layer top, by various definitions, from a large set of GPS dropsonde data within the hurricane core, and found that the well-mixed layer is typically about half the depth of the inflow layer, but that the use of a Richardson-number criterion (different from that in MRF) gave an intermediate height. These differences in the diagnosed boundary-layer height would have a significant impact on the diffusivity.

Here h is prescribed as an external parameter. The diffusivity above h is set to $1\,\mathrm{m^2 s^{-1}}$ (a small value) for numerical stability.

[5] Louis (1979) contains a typographical error in the equation for $f(\mathrm{Ri})$, corrected in Louis et al. (1982).

[6] Rossby-number similarity theory (Garratt 1992, p 44) implies $u_*/|f|$ is the depth scale for a neutral boundary layer. In a tropical cyclone, f should be replaced with the inertial stability I so, to the extent that the boundary-layer depth influences l, a shorter length scale may be appropriate.

d. Higher-order closure

Higher order closures carry additional prognostic equations for turbulence quantities. In their simplest form, the TKE is predicted, and other turbulence quantities are diagnosed from the TKE and either a mixing length or the prognosed turbulence dissipation. The mixing length equation, where used, may be either diagnostic or prognostic. The example of a higher-order closure used in this study will be the Mellor-Yamada level $2\frac{1}{4}$ scheme (Galperin et al. 1988) as implemented by KW01. The prognostic turbulence quantity is the square root of twice the TKE,

$$q = (u'^2 + v'^2 + w'^2)^{1/2}, \tag{16}$$

and the mixing length l is diagnosed from Blackadar's equation (8) with some additional stability constraints. The prognostic TKE equation includes parameterisations of the shear generation, buoyant generation/destruction, turbulent transport, and dissipation. In contrast to some higher-order closures, vertical and horizontal advection of q is included. The diffusivities are given by

$$K_m = lqS_M \tag{17}$$

$$K_h = lqS_H \tag{18}$$

where S_M and S_H are functions of the dimensionless shear and virtual potential temperature gradients given by Galperin et al. (1988). As well as the full level $2\frac{1}{4}$ scheme, we will also use a neutral version, derived by setting the buoyant production to zero in the TKE equation, and removing the stability dependences from S_M, S_H and l.

Examples of higher-order closures used in tropical cyclone simulation include the Mellor-Yamada schemes in MM5 and WRF, the Burk-Thompson and Gayno-Seaman schemes in MM5, and the modified scheme of Langland and Liou (1996) in TCM-4 (Wang 2007). Although these schemes are here classified together, they can contain significant differences. For example, the latter uses a prognostic equation for the turbulence dissipation rate instead of a length scale equation.

e. Which schemes are in common use?

To confirm that the preceding schemes represent those typically used for tropical cyclone simulation, and also to discover their relative frequency of use, the recent literature was surveyed. All articles published in *Monthly Weather Review*, *The Journal of the Atmospheric Sciences*, and *The Quarterly Journal of the Royal Meteorological Society* during 2006 – 2010 that presented simulations of tropical cyclones using either MM5 or WRF were examined, and the boundary layer parameterisation identified. Articles which used more than one scheme were counted for each, and follow-up articles, including multi-part papers, were treated as separate papers. The results are summarised in Table 2.

This survey showed, firstly, that the preceding discussion of boundary-layer parameterisations is representative of current practice in tropical cyclone simulation; all the papers surveyed used a scheme of one of these types. Secondly, in MM5, the Bulk and Hi-Res schemes, which here are considered together as they use the same diffusivity parameterisation, are substantially the most popular, representing 72% of the papers surveyed. The KPP scheme has similar usage to the combined higher-order schemes, but these substantially trail the Bulk/Hi-Res schemes. In WRF, the situation is quite different. Over three-quarters of papers use a KPP parameterisation, with most of these using the YSU scheme. The remainder use a Mellor-Yamada schemes.

4. The Model

We use KW01's model, modified to include the turbulence parameterisations discribed above, and with improved numerics (Appendix A). This model diagnoses the boundary layer flow by solving the dry equations of motion beneath a prescribed pressure field representative of a tropical cyclone. The solution is found by integrating the equations forward in time until a quasi-steady state is achieved; in practice the 24 hours used is more than sufficient. The model is fully three-dimensional but is here applied only to stationary storms and so is effectively two-dimensional (radius-height). All results were transformed to storm-centred cylindrical coordinates, and azimuthally averaged to remove weak spiral-band features that are presumably due to an instability similar to those discussed by Nolan (2005) and Foster (2005), prior to further analysis. The boundary-layer does not modify the prescribed pressure at the model top, so the model represents one side of what in reality is a two-way interaction between the boundary-layer and the rest of the cyclone. In all the runs presented, there are 20 levels with the lowest at 10 m and the top at 2.25 km; resolution is highest near the surface. The horizontal grid-spacing is 3 km.

5. Results

We now present a series of simulations with the KW01 model, using each representative parameterisation in turn. In each case, the upper boundary con-

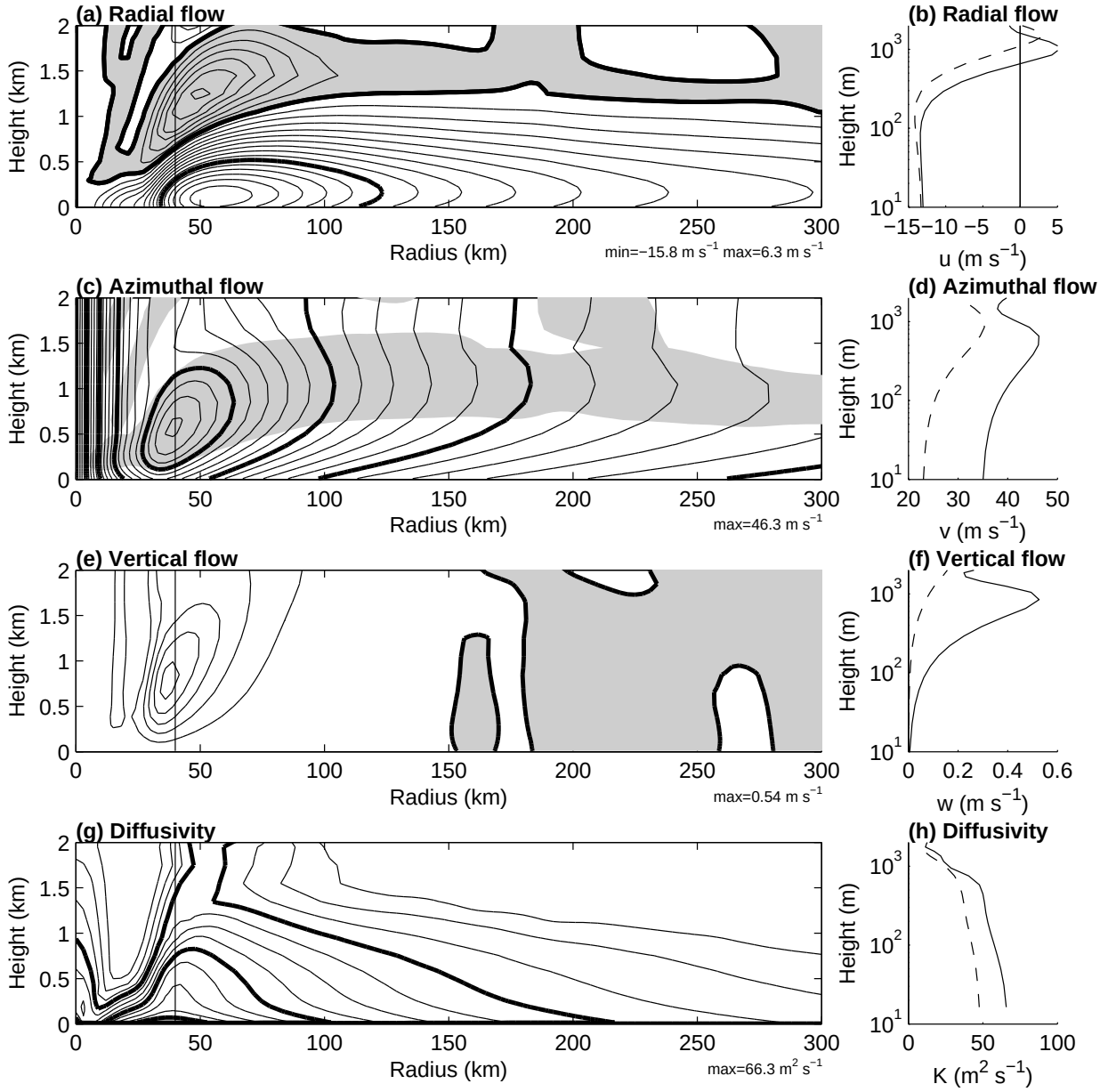

FIG. 2. Simulated flow using the MM5 Bulk scheme. Left column: Radius-height contour plots of (a) radial flow, (c) azimuthal flow, (e) vertical flow, and (g) turbulent diffusivity. Right column: Vertical profiles at the RMW (solid) and twice the RMW (dashed) of, (b) radial flow, (d) azimuthal flow, (f) vertical flow and (h) turbulent diffusivity. Contour intervals are as follows: (a), 1 m s^{-1}, multiples of 10 m s^{-1} shown bold, outflow shaded; (c), 2 m s^{-1}, multiples of 10 m s^{-1} shown bold, regions where the flow is supergradient shaded; (e), 0.1 m s^{-1}; 0 shown bold, downwards motion shaded; (g), 5 $m^2 s^{-1}$, multiples of 20 $m^2 s^{-1}$ shown bold. The text below panels a, c, e and g indicates the values of those extrema over the domains 15 km $< r <$ 300 km, $0 < z <$ 2 km.

TABLE 2. Boundary-layer schemes used in articles that presented tropical cyclone simulations using MM5 or WRF in three prominent journals published from 2006 to 2010, as detailed in the text. The upper row for each model shows the raw numbers, and the lower row the frequency. The frequencies add up to more than 100% because some papers considered more than one scheme. Column heading abbreviations are BT: Burk-Thompson, GS: Gayno-Seaman, MY: all Mellor-Yamada schemes, MRF: Medium-Range Forecast, YSU: Yonsei University, NS: not specified. The "not specified" category was ignored in calculating the frequencies.

	Bulk	Hi-Res	BT	GS	MY	MRF	YSU	NS	No of papers
MM5	10	32	3	1	7	10	—	6	64
	17%	55%	5%	2%	12%	17%			
WRF	—	—	—	—	13	2	37	7	55
					27%	4%	77%		

dition to the model is provided by a Holland (1980) parametric profile with a maximum gradient wind of 39.1 m s^{-1} at a radius of 40 km, and a B parameter of 1.3, modified within the radius of maximum winds as described by KW01. The vortex is stationary. The gradient wind field is thus identical to that of vortex I of KW01.

a. The Bulk and Hi-Res schemes

Figure 2 shows radius-height sections of the radial, azimuthal and vertical velocities, and the momentum diffusivity for our implementation of these schemes, along with vertical profiles of these quantities at once and twice the RMW. The inflow depth increases gradually inwards to about 150-km radius, before decreasing sharply towards the centre. Peak inflow is 15.8 m s^{-1}, and is surmounted by an outflow layer with maximum 6.3 m s^{-1}. The azimuthal flow is supergradient in the upper part of the inflow layer and lower part of the outflow layer, as indicated by the shading in panel c. The azimuthal wind maximum is 46.3 m s^{-1}, in the upper part of the inflow layer near the RMW. The strongest updraft is 0.54 m s^{-1} just inside of the RMW, and there is weak subsidence outside of about 150-km radius. The diffusivity is a maximum at the lowest model level, and is largest near the RMW, as in the simulations with these schemes shown in Braun and Tao (2000) and Smith and Thomsen (2010). Both of these trends are due to the distribution of vertical wind shear. In addition, the diffusivity shows a small upwards extension coincident with the peak updraft.

The vertical profiles of azimuthal flow (Fig. 2d) and wind speed (not shown) show that the near-surface flow does not follow a logarithmic profile; instead it has a nearly linear variation with height in the lowest 200 m. Observations (Powell et al. 2003) show that the logarithmic profile should extend to at least 200-m height. This deficiency is as expected; the discussion in section 3a showed that taking l constant with height leads to a linear, rather than logarithmic, near-surface variation of wind with height.

b. The Louis scheme

Results from this scheme are presented by the black contours in Fig. 3. Recall that the differences between this scheme and the Bulk/Hi-Res scheme include the use of Blackadar's length scale (8) in place of constant l. The inflow layer is somewhat deeper at large radii than in the Bulk/Hi-Res scheme, and the inflow and azimuthal wind maxima are markedly weaker. The azimuthal flow near the top of the inflow layer is generally less strongly supergradient, and the outflow layer aloft is much weaker. The peak updraft is markedly weaker and occurs at larger radii, and the radius of transition to a downdraft is slightly reduced. The radial distribution of K is similar, but the vertical distribution is very different, with the maximum occurring near the middle of the inflow layer, rather than at the surface. There is a small upwards extension of higher values of K just outside of the RMW, coincident with the main updraft, similar to that with the Bulk/HiRes scheme. The diffusivity maximum near $r = 0$ is due to the combination of very weak shear with slight static instability in this region, leading to large negative Ri and hence a large $f(\mathrm{Ri})$ term in (10).

Examination of the vertical profiles in Fig. 3b,d shows that the azimuthal flow and wind speed (not shown) follow logarithmic profiles up to about several hundreds of metres height, while the depth of the logarithmic profile for the radial flow is somewhat shallower. These profiles are thus consistent with observations. The azimuthal component of the stress actually varies substantially across the approximately logarithmic layer (not shown), emphasising that constant flux is sufficient, but not necessary, for a near-logarithmic profile. The reason for the different depth

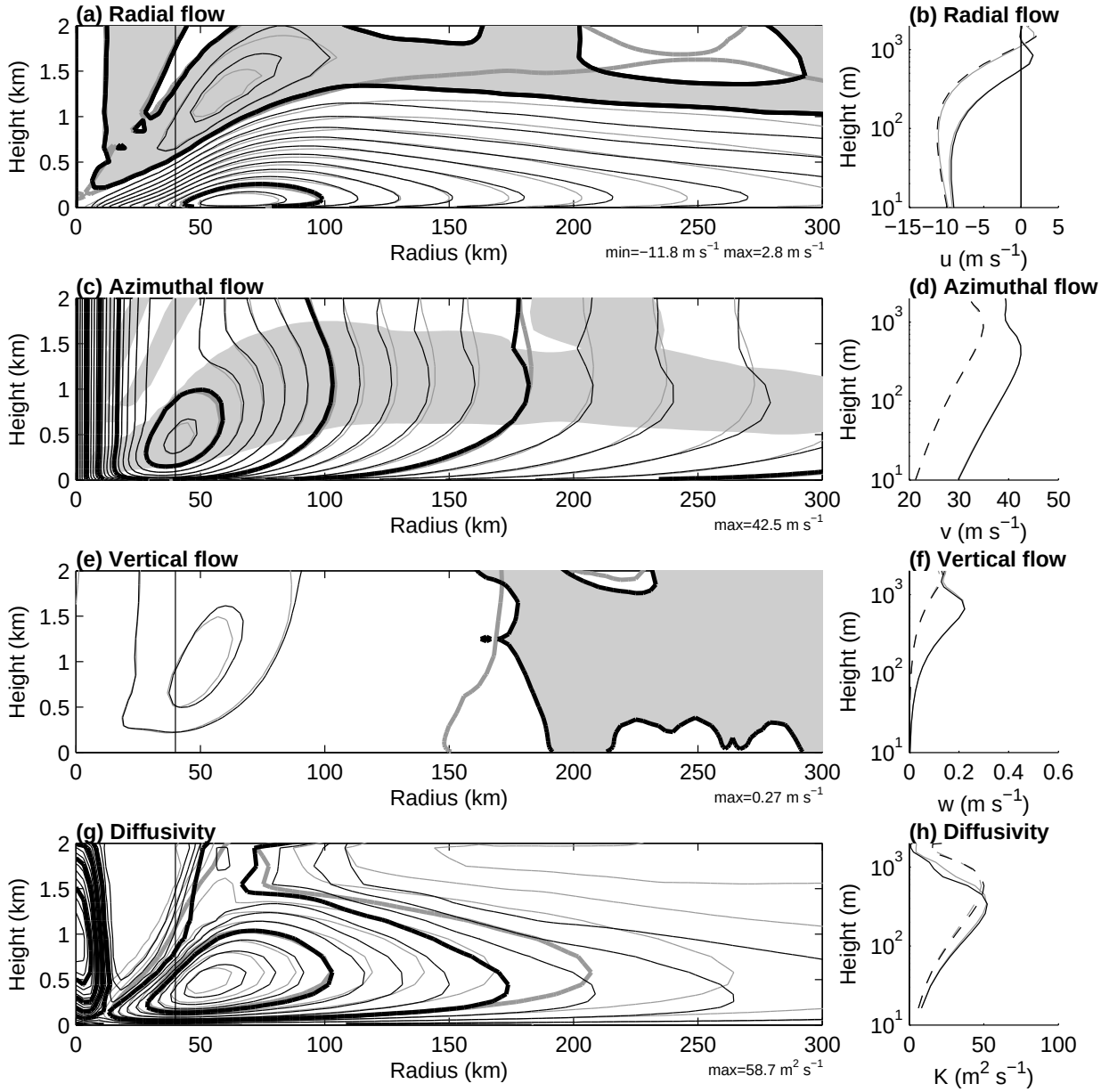

FIG. 3. As for Fig. 2, except for the Louis scheme. The grey contours and curves are for the neutral version of the Louis scheme.

of the logarithmic layer between the two wind components is that the cross-stream stress reaches zero at a much lower height than the along-stream stress (Garratt 1992, Fig. 3.3), so the height to which the stress component can be assumed to be close to its surface value is less for the radial component than for the azimuthal. The lack of horizontal homogeneity may also play a role, especially near the RMW.

The grey contours in Fig. 3 shows results from the Louis-neutral scheme. Within the lower half of the inflow layer in the area of ascent, the results are nearly identical. Above that, the diffusivity is somewhat larger in the neutral scheme due to the neglect of the effects of the stable stratification. This increased mixing leads to a smoother wind field in that region. At larger radii, subsidence has increased the static stability and suppressed K in the Louis but not the Louis-neutral scheme. The latter therefore has more mixing and a deeper inflow layer. The maximum in K near $r = 0$ has disappeared, due to the removal of its stability dependence.

We are here using a smaller value of the asymptotic mixing length, $l_\infty = 80\,\mathrm{m}$, than the 150 m recommended in Louis et al. (1982), for consistency with our higher-order closure scheme. The results of Zhang et al. (2011b) may also justify a higher value. Simulations with l_∞ ranging from 40 to 300 m (not shown) revealed that increasing l_∞ leads to higher diffusivity in the middle to upper part of the inflow layer. The increased mixing more effectively transfers azimuthal momentum downwards, so the near-surface azimuthal flow is stronger. The surface inflow weakens, mainly because the stronger near-surface azimuthal flow results in a reduced inwards-acting residual between the pressure-gradient, centrifugal and Coriolis forces. However, the depth of the inflow layer increases, mainly because K has increased and the height scale for the tropical cyclone boundary layer is

$$\delta = \sqrt{\frac{2K}{I}} \tag{19}$$

(Rosenthal 1962; Eliassen and Lystad 1977; Kepert 2001). Here the inertial stability I is defined by $I^2 = (f+2V/r)(f+V/r+\partial V/\partial r)$, where V is the gradient wind speed. Reducing l_∞ reverses the above effects; the near-surface azimuthal flow weakens, the inflow strengthens and the inflow layer becomes shallower.

c. Non-local KPP closure.

Figure 4 shows a simulation with the nonlocal KPP-closure, in which the diffusivity profile top was set to $h = 1.5\,\mathrm{km}$ everywhere; this value was chosen as being close to the inflow depth in much of the domain of the preceding two simulations. The inflow layer is mostly close to h when $r > 80\,\mathrm{km}$, but reduces in depth for smaller r. This decrease is due to the increase in inertial stability at inner radii, and that the height scale for the tropical cyclone boundary layer is given by (19). The inflow and supergradient flow are generally weaker than with either the Bulk and Louis schemes, because the diffusivity is larger. The larger diffusivity more efficiently mixes azimuthal momentum down to the surface, replacing that lost to surface friction, and thereby reducing the gradient imbalance in the lower boundary layer. Thus the inwards-acting residual between the centrifugal, Coriolis and pressure gradient forces is smaller here, and is the main reason for the weaker inflow. Near the surface, $K \approx ku_*z$ and the azimuthal wind profile is logarithmic.

Several radially-constant h were tested. Values significantly smaller than $h \lesssim 1\,\mathrm{km}$ led to extreme supergradient winds at the eyewall, very strong outflow above h, a very strong eyewall updraft, and made the boundary layer too shallow at large radii. On the other hand, increasing h leads to higher values of K through (14) and (15) and a deeper inflow layer. The departure from gradient balance, strength of the near-surface inflow, maximum updraft, and strength of the outflow layer all diminish when h is increased. However, the depth of the inflow layer increases only modestly in the inner core, consistent with the scaling with δ. Increasing h makes the simulation even more like those of Braun and Tao (2000) and Smith and Thomsen (2010) with the MRF parameterisation. We therefore suspect that the diagnosed boundary-layer height in their simulations is too high, and agree with Noh et al.'s (2003) conclusions regarding this aspect of the MRF scheme.

Comparing Fig. 4g,h to Fig. 3g,h, it is apparent that the diffusivity maximum is generally at a similar height at most radii to that in the Louis scheme, but its magnitude is much larger. This large diffusivity is responsible for the stronger mixing and reduced surface inflow and eyewall updraft, and was found by Braun and Tao (2000) to cause an excessively dry boundary layer and thereby reduce the storm intensity. We performed a range of tuning experiments to better specify K. Using a smaller h to reduce K leads to unrealistic simulations; for example, with $h = 800\,\mathrm{m}$ the inflow layer is too shallow, and the outflow layer aloft is too strong, peaking at $10\,\mathrm{m\,s^{-1}}$. It was therefore necessary to change p also. Figure 5 shows a simulation in which $p = 4$ and h increases linearly with radius from 50 m at $r = 0$ to 2.5 km at $r = 50\,\mathrm{km}$, and is then constant. This prescription was chosen since it mostly retained the height

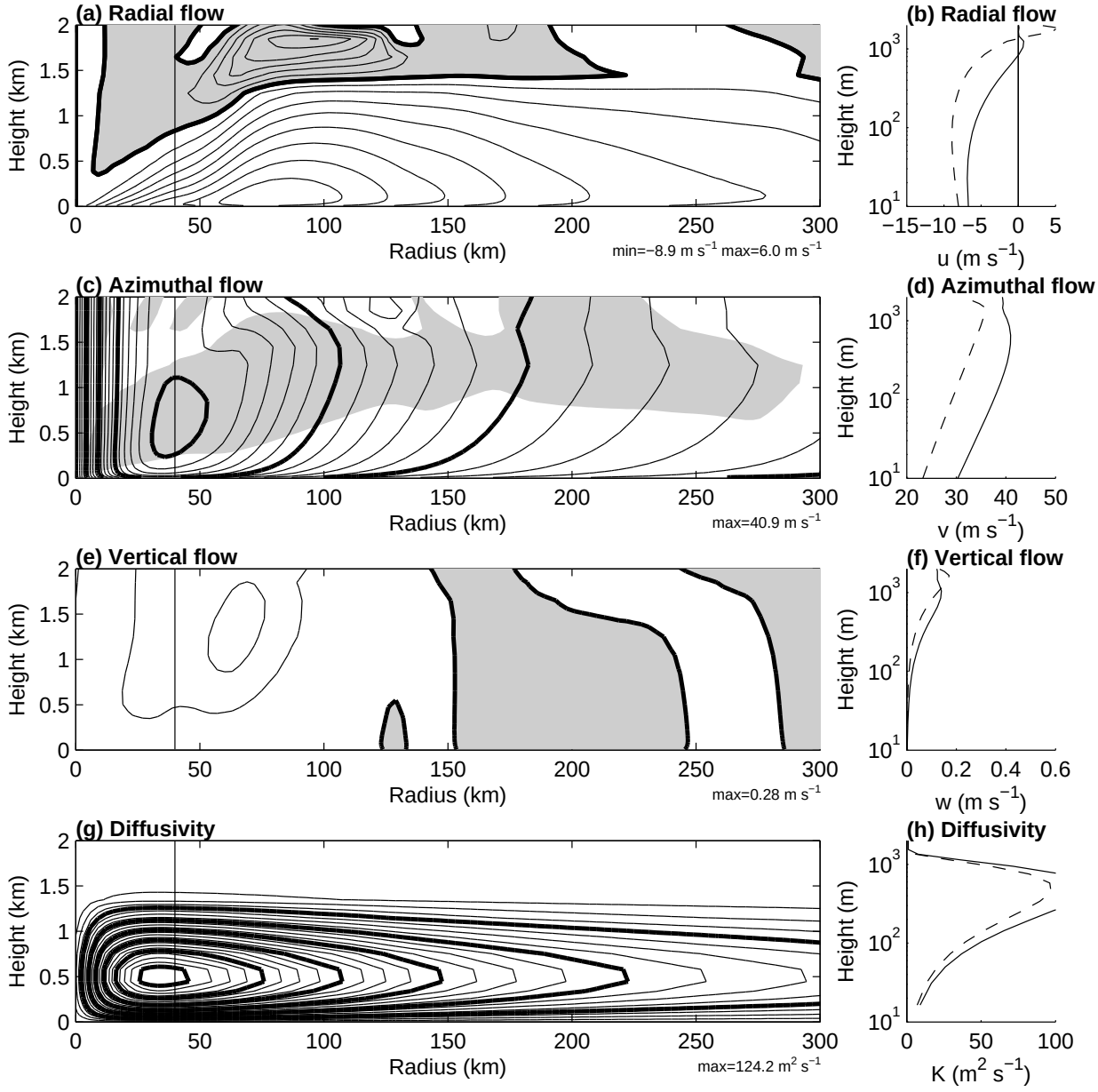

FIG. 4. As for Fig. 2, except for the nonlocal KPP closure with fixed $h = 1.5\,\mathrm{km}$ and $p = 2$.

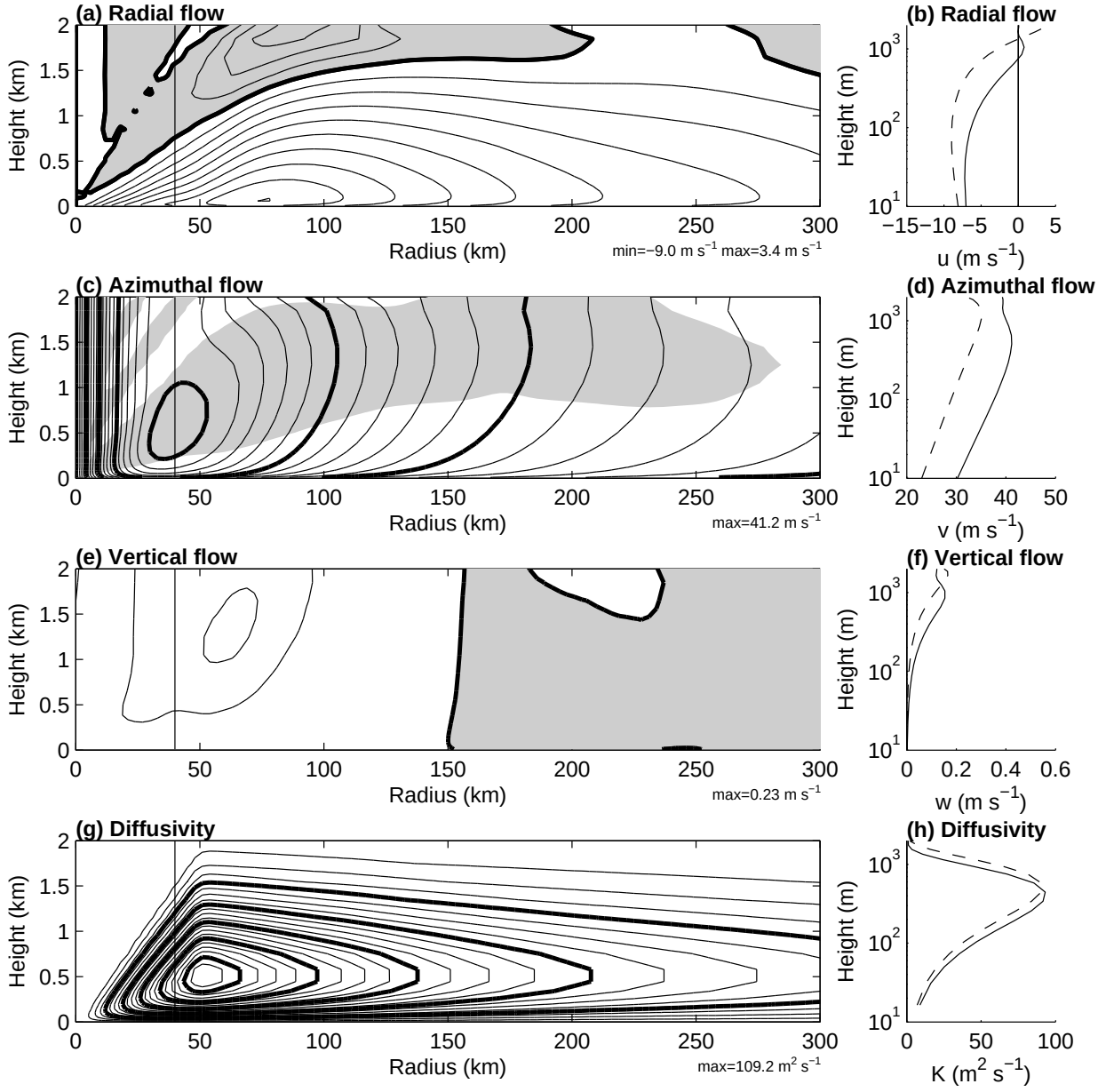

FIG. 5. As for Fig. 2, except for the nonlocal KPP closure with h varying with radius and $p = 4$.

of the maximum in K, but substantially reduced its amplitude to roughly twice that in the Louis-neutral scheme. The diagnosed flow structure is closer to that from the Louis-neutral scheme, although the magnitudes remain closer to those in Fig. 4.

The KPP closure used here is simpler than commonly-used examples of such schemes in several respects. In particular, compared to the YSU scheme in WRF (Hong et al. 2006), it (i) omits parameterisation of the countergradient fluxes, (ii) uses a constant K for $z > h$ rather than a local closure, (iii) omits explicit parametisation of the entrainment flux, (iv) takes the turbulent Prandtl number to be 1, and (v) assigns h as an external parameter. Additional simulations were performed with some of these simplifications removed. Including countergradient fluxes as in Hong et al. (2006) slightly reduces the inflow-layer depth and slightly strengthens the near-surface inflow, but does not substantially affect the simulation. Using the Louis scheme for $z > h$ increases K there and substantially reduces the strength of the outflow layer from that shown in Fig. 4. Increasing K near and above h to account for entrainment is expected to have a similar effect. The turbulent Prandtl number is not substantially different to 1 in the higher-order closure, and is less relevant to this study as we do not discuss the thermal structure, so this factor was not tested. Lastly, when h was calculated interactively as in Hong et al. (2006), the diagnosed depth was near 2 km. The flow was similar to that in Fig. 4, except that the boundary layer was deeper (consistent with larger h and hence K) and that the vertical gradients in the upper part of the domain were weaker. However, we caution that, although the same method was used to diagnose h as in Hong et al. (2006), the results here may be different to those obtained with a full model using that scheme because the present model omits the effect of cloud processes; in particular, convective downdrafts may cool the boundary layer and lead to a lower diagnosed h than here.

d. Higher-order closure

Figure 6 shows the results from the Mellor-Yamada level $2\frac{1}{4}$ scheme; the black contours show the full scheme and the grey contours the neutral equivalent. The fields are quite similar to those obtained using the Louis scheme, especially in the innermost 200 km. The chief differences in this region are that the maximum updraft is a little stronger and the diffusivity a little weaker than in the Louis scheme. Note that the upwards extension of the diffusivity just outside of the RMW is present here also, as is the maximum near $r = 0$. In the innermost 200 km the differences between the full and neutral versions of the scheme are similar to those with the Louis scheme.

	Bulk/HiRes	K=50	KPP h=1.5km	KPP vary h, p=4	K=ku_*l	Louis neutral	Louis	MY TKE neutral	MY TKE
Bulk/HiRes		1.3	2.6	2.5	2.0	1.9	1.9	1.9	1.8
K=50	0.7		1.6	1.6	1.4	1.4	1.5	1.4	1.6
KPP h=1.5km	1.5	1.0		0.2	1.1	1.2	1.3	1.2	1.4
KPP vary h, p=4	1.4	0.9	0.1		1.0	1.0	1.1	1.0	1.3
K=ku_*l	1.2	0.9	0.5	0.5		0.2	0.4	0.2	0.6
Louis neutral	1.2	0.9	0.6	0.5	0.1		0.3	0.0	0.6
Louis	1.1	0.9	0.6	0.6	0.3	0.2		0.3	0.3
MY TKE neutral	1.2	0.9	0.6	0.5	0.1	0.0	0.2		0.6
MY TKE	1.1	0.9	0.6	0.6	0.3	0.2	0.1	0.2	

FIG. 7. RMS differences in $\mathrm{m\,s^{-1}}$ between various parameterisations, area-weighted in the r–z plane for $r < 300\,\mathrm{km}$ and $z < 1\,\mathrm{km}$. Numbers above the diagonal refer to the radial component, and below to the azimuthal component, of velocity. The intensity of the shading is proportional to the values.

The radius at which ascent transitions to subsidence is somewhat larger with this parameterisation than with the Louis scheme, and the inflow layer in the region of descent is shallower, with a more sharply defined top. Subsidence increases the stability, which destroys TKE and reduces the diffusivity, leading to a shallower boundary layer. This effect is stronger with the higher-order closure than with the Louis scheme.

As with the Louis and nonlocal schemes, the profiles of azimuthal velocity and wind speed are close to logarithmic up to several hundreds of metres in height, while the radial wind has a somewhat shallower logarithmic layer.

6. Discussion

RMS differences of the radial and azimuthal flow between all pairs of parameterisations, area-weighted in r-z space for $r < 300\,\mathrm{km}$ and $z < 1\,\mathrm{km}$, are shown in Fig. 7. This figure includes also simulations with the simple mixing length parameterisation of Kepert (2010a), in which $K = ku_*l$ and l is given by (8), and with constant $K = 50\,\mathrm{m^2 s^{-1}}$ to facil-

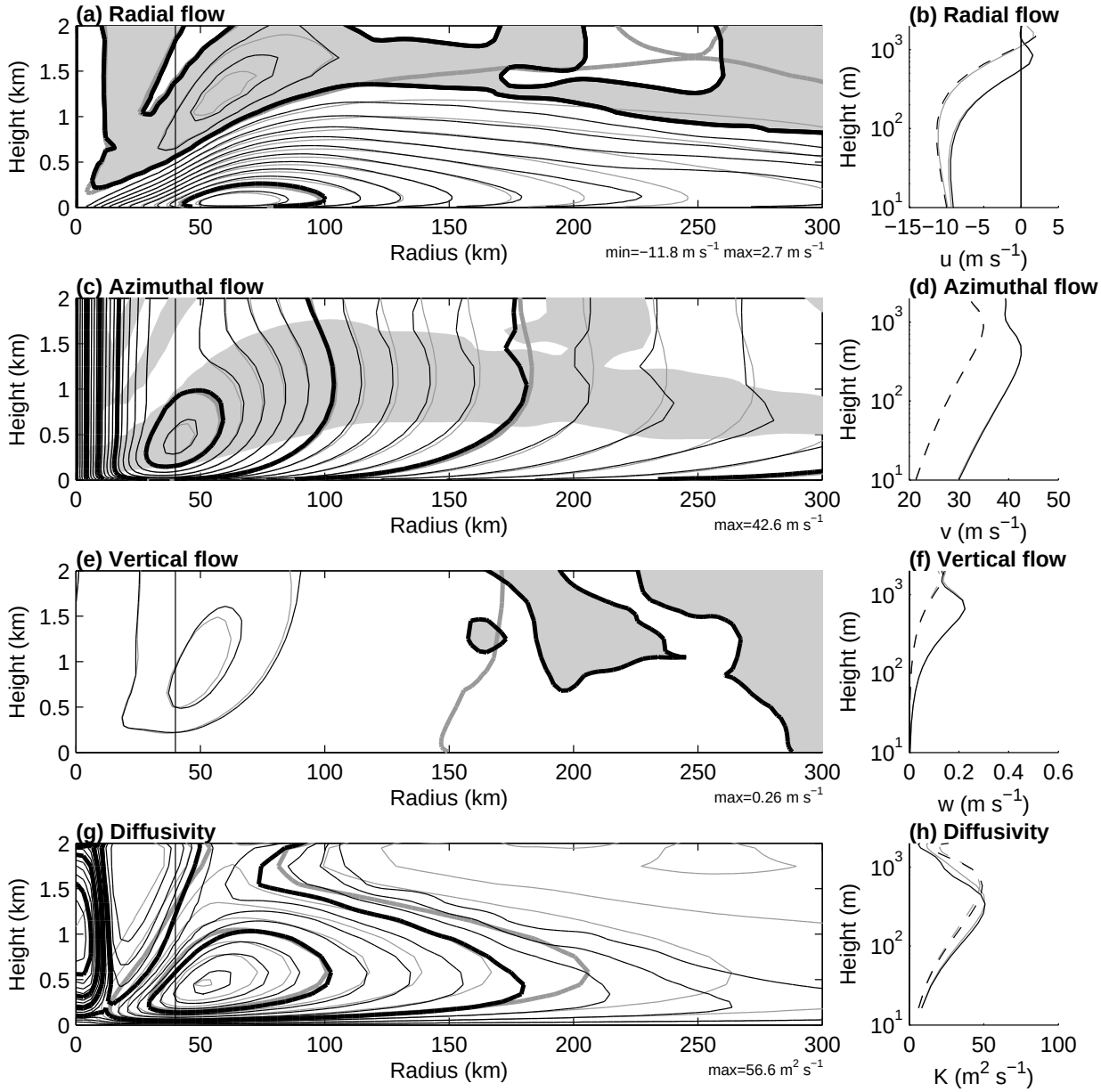

FIG. 6. As for Fig. 2, except for the Mellor-Yamada level 2.25 scheme. The grey contours and curves are for the neutral version of this scheme.

itate comparison with Foster's (2009) results. The simple mixing-length parameterisation gives similar values of K to the Louis and higher-order closure schemes near the surface, but does not diminish K towards and above the top of the inflow layer and therefore would not be suitable in a full model; it differs from the neutral Louis scheme by using the surface-layer shear rather than the local shear, and can therefore be regarded as a nonlocal closure. The table confirms the differences seen in the previous section; most of the schemes in which $K \approx ku_*z$ near the surface produce quantitatively similar results (i.e. the simple mixing length scheme, and the Louis and Mellor-Yamada schemes), with the exception of the KPP closure where the the shape of the profile with $p = 2$ causes excessive mixing, even with a realistic h. The schemes which violate the near-surface condition $K \approx ku_*z$ (the Bulk/Hi-Res scheme and the use of $K = 50\,\mathrm{m^2 s^{-1}}$), are quite different from those that conform to it and from each other. The latter difference arises because these parameterisations also give quite different diffusivities above the surface layer.

The differences between the parameterisations found here are consistent with those noted by Braun and Tao (2000) and by Smith and Thomsen (2010). The Bulk and Hi-Res (often called Blackadar) schemes have the strongest surface inflow and strongest supergradient winds in their simulations and in those presented here. While these authors do not present height profiles of wind, examination of their contour plots shows that the contours of azimuthal velocity are nearly straight in the lowest few hundred metres with these schemes, but distinctly curved with the others. The same phenomenon is seen in Fig. 2c compared to Figs. 3c to 6c; hence we conclude that their simulations with these parameterisations produced a linear, rather than logarithmic, near-surface layer.

There is quite close agreement between the Louis and the level $2\frac{1}{4}$ schemes. We caution against regarding these schemes as being independent, since it is possible to derive the neutral version of the Louis scheme from the neutral version of the level $2\frac{1}{4}$ scheme (Appendix B). However, we prefer these schemes to KPP schemes even if the boundary-layer depth is diagnosed correctly, since these schemes are based on physical principles while the KPP scheme fits an arbitrary polynomial to conditions at the top and bottom of the boundary layer. That is not to say, of course, that the Louis and Mellor-Yamada schemes are free of empiricism; in particular, the asymptotic mixing length l_∞ is uncertain and the simulated flow is sensitive to this parameter as discussed in section 5b.

Three of the four parameterisations considered here showed a lobe of diffusivity extending above the inflow layer, coincident with the peak updraft. Smith and Montgomery (2010) attributed a similar feature in their simulations to lofting of TKE in the updraft, but that explanation cannot apply here because the Bulk/Hi-Res and Louis schemes do not predict TKE, let alone advect it. Rather, the lobe is produced *in situ* by a combination of the strong radial wind-shear near the inflow-layer top and reduced static stability in the updraft. Note that a model with moist processes would be expected to have even larger diffusivity in this region, since condensation-induced buoyancy would also generate turbulence. We surmise that the high TKE that Lorsolo et al. (2010) found in the eyewall is predominantly generated in situ by buoyancy.

The role of TKE advection was also considered by Nolan et al. (2009b), who proposed that the excess dissipation of momentum when using a higher-order scheme (the Mellor-Yamada-Janjić scheme, Janjić 1994) in WRF was because that implementation omitted the advection of TKE. To test this, we reran our simulation with the higher-order closure, but with the TKE advection turned off. The resulting wind field was virtually unchanged from that shown in Fig. 6, although there were minor changes in the diffusivity and TKE. It therefore appears that some factor other than the omission of TKE advection was responsible for the differences that Nolan et al. (2009b) noted.

Braun and Tao (2000) found that the MRF scheme, an example of a nonlocal KPP closure, produced too deep and too strong mixing, while Smith and Thomsen (2010) similarly noted that this scheme produced excessive mixing. Their simulations featured weak inflow and a relatively broad wind maximum, while those presented here featured at least the first of these characteristics and other experiments with greater h had the second as well (not shown). It seems from our simulations and their figures that the primary cause of the excessive mixing is that the diagnosed boundary-layer depth in this scheme is too high[7]. However, a simulation with a reasonable $h = 1.5\,\mathrm{km}$ still gave substantially larger K than either the Louis or higher-order closure schemes in the outer part of the storm, even though the inflow depths were similar. Some experimentation showed that a somewhat closer match could be achieved by increasing the

[7]Note that in Braun and Tao (2000) and Smith and Thomsen's (2010) simulations, the storm is less intense with a larger RMW when the MRF scheme is used, leading to a smaller inertial stability at the RMW with a slightly increased inflow-layer depth through (19). However the excess diffusivity seems to be the dominant effect.

shape parameter to $p = 4$ and prescribing a radially-varying h. Obviously this is a fairly drastic change to propose, and would likely upset the performance of the scheme in situations where it is now satisfactory. At best, it would need substantial retuning.

In this context, it is interesting to consider the comparison by Nolan et al. (2009a,b) of two PBL schemes, a higher-order closure (the Mellor-Yamada-Janjić scheme, Janjić 1994) and a nonlocal closure (the YSU scheme). The YSU scheme has several differences from the MRF, including the treatments of entrainment at an inversion and the countergradient heat flux, but most importantly here, its method of calculating h. In contrast to Braun and Tao (2000) and Smith and Thomsen (2010), Nolan et al. found similar performance from the higher-order closure and nonlocal schemes, suggesting that the new method of calculating h in the YSU scheme is an improvement.

The simulations presented in section 5 were repeated for two other parametric tropical cyclone profiles; an intense storm (maximum gradient wind $59.4\,\mathrm{m\ s^{-1}}$ at 30-km radius, $B = 1.5$) and a marginal storm (maximum gradient wind $19.1\,\mathrm{m\ s^{-1}}$ at 50-km radius, $B = 1.1$). In both cases, the relative performance of the various parameterisations were similar to those shown:

- The Bulk/HiRes parameterisation produced the strongest inflow and updraft, most strongly supergradient winds (11% in the weak storm, and 27% in the strong), had a near-surface diffusivity maximum and failed to produce a logarithmic surface layer.
- The Louis and higher-order closures produced very similar results, with peak winds that were moderately supergradient (7% in the weak storm, and 13% in the strong), and weaker inflow and eyewall updraft than the Bulk/HiRes parameterisation.
- The KPP closure produced the highest diffusivities, the weakest inflow, updraft and supergradient flow, and a logarithmic surface layer.

Thus the main conclusions from this study appear to be robust with respect to storm intensity.

7. Conclusions

The diagnostic tropical cyclone boundary layer model of KW01 was extended to include implementations of several different turbulence parameterisations, representative of those commonly used in tropical cyclone modelling. The differences in the simulations are similar to those found by previous authors, including Braun and Tao (2000), Smith and Thomsen (2010) and Foster (2009). The simulations presented here differ from the first two of those earlier works by having imposed an identical structure of the cyclone above the boundary layer, rather than simulating the whole storm. This approach has the advantage of being able to isolate the direct effects of the parameterisation from indirect effects in which the boundary layer modifies the overall structure of the storm. We thus conclude that a substantial reason for the differences between the simulations that those authors found was the direct effects of the PBL parameterisation. However, the boundary layer parameterisation does have an effect on the structure of the cyclone as a whole, as shown by the variations in central pressures and radii of maximum winds noted by those authors, and by the flow differences between our simulations being smaller than they found. That is, the feedback between the boundary layer and the rest of the storm discussed in the introduction is present.

One class of schemes, representing the Bulk and Hi-Res parameterisations available within MM5, produces the strongest surface inflow, strongest supergradient jet, and fails to produce the observed near-surface logarithmic layer. These schemes also produce substantially the largest non-linear terms in analyses of the momentum budget similar to that in Kepert (2010b) (not shown). These features are due to the diffusivity being a maximum at the lowest model level, which in turn is due to an incorrect parameterisation of the mixing length. These schemes are therefore significantly in error on observational and theoretical grounds. Examination of the literature documenting these parameterisations suggests that this error arose because the Blackadar (1976) scheme, intended only for the nocturnal boundary layer, was implemented more broadly, without the modifications that its author had recommended for such use. As the Bulk and Hi-Res schemes fail to replicate observations and violate theoretical expectations, it is recommended that they not be used for tropical cyclone simulation. Of course, the logarithmic surface layer occurs much more widely than just within tropical cyclones. Although we have not tested these schemes in other situations, we expect that the problems identified in tropical cyclones will also occur elsewhere, so these schemes are probably unsuitable for many other applications.

The failure to produce a logarithmic surface layer is expected to affect the simulation of the rest of the storm, and should not be regarded as being of concern only to boundary-layer meteorologists. In particular, this failure leads to systematic biases in the lowest

model level wind, temperature and humidity fields, and hence in the surface fluxes. It thus has a direct impact on the final intensity and on the intensification of the modelled storm.

A survey of the recent tropical cyclone literature found that a large proportion of papers used either the Bulk or Hi-Res schemes, with almost three-quarters of MM5 papers being in this category. Some of these papers contained major conclusions about the role of the boundary layer in tropical cyclone dynamics. For example, Smith et al. (2009) argue that radial convergence in the boundary layer intensifies the inner core of the storm, a mechanism they claim is likely enhanced by the development of supergradient winds there. However, their calculations used the MM5 Bulk boundary-layer parameterisation, which we have shown leads to an excessively strong inflow and updraft, thereby exaggerating both the inwards advection of angular momentum within the inflow layer, the strength of the supergradient flow, and the rate at which it is advected upwards. They discuss also the overshoot of the inflow beneath the eyewall, but this overshoot depends partly upon the $u\partial u/\partial r$ term in the radial momentum equation, the peak magnitude of which occurs near the surface and inwards of the inflow maximum, and is at least three times larger with the Bulk/Hi-Res scheme than in the other parameterisations presented here. It would therefore seem prudent that such studies be repeated with a more reasonable parameterisation.

Nonlocal closure schemes of the KPP type are sensitive to their diagnosis of the boundary layer depth. Defining the boundary-layer depth in the tropical cyclone core is not straightforward (Kepert 2010a; Smith and Montgomery 2010) and observations show that different definitions can yield markedly different results (Zhang et al. 2011b). Nonlocal KPP closure schemes can perform satisfactorily, as shown for the YSU scheme by Nolan et al. (2009a,b), or poorly, as found for the MRF scheme by Braun and Tao (2000) and Smith and Thomsen (2010). While there are several differences between the YSU and MRF schemes, the most important in the present context seems to be the different methods used to determine h. Even if h is set to an inflow depth consistent with that from the Louis or higher-order closure schemes, much greater mixing occurs with the usual shape parameter $p = 2$. We therefore recommend that such schemes be used with caution. As a minimal precaution, the boundary-layer depth should be checked to ensure that reasonable values are being diagnosed.

The Louis PBL scheme and higher-order closure here produced very similar results, with the main difference being the latter's greater sensitivity to subsidence-induced stabilisation above the boundary layer in the outer part of the cyclone. Both correctly produce a logarithmic wind profile near the surface, while the higher-order closure scheme used has been previously shown to produce a satisfactory match to observations in this model (Kepert 2006a,b; Schwendike and Kepert 2008). The main difference relevant to tropical cyclone simulation between the Louis and Bulk/Hi-Res schemes is the former's use of the Blackadar (1962) length scale rather than a constant; this difference is directly responsible for the logarithmic profile. The Louis scheme is significantly less expensive to calculate than a higher-order closure, so may be the preferred choice if computational resources are constrained.

On the basis of these results and because they produce a near-surface logarithmic layer, we recommend either the Louis or Mellor-Yamada schemes as being suitable for tropical cyclone simulation. We do caution against regarding these schemes as providing independent pieces of evidence; in particular we show in Appendix B that under neutral conditions, the Louis scheme is equivalent to a simpler version of the Mellor-Yamada scheme. However, since the diffusivity in these schemes is based on physical principles, while that in the KPP schemes uses an arbitrary polynomial fit to conditions at the bottom and top of the boundary layer, we prefer these schemes to the MRF and YSU schemes.

More definite recommendations would require an extensive quantitative comparison with observations. The boundary layer structure, including the inflow angle and degree of supergradient flow, is sensitive to the storm structure (Kepert and Wang 2001; Kepert 2006a,b; Schwendike and Kepert 2008); specifically to the radial distribution of absolute angular momentum or, equivalently, the inertial stability. Such a comparison would need to diagnose this quantity for each storm and would therefore be an extensive undertaking, beyond the scope of this paper. However, it would be beneficial since it would also help reduce uncertainties, such as the choice of asymptotic mixing length, in these schemes.

Acknowledgments.

This work was partially supported by the U.S. Office of Naval Research, under award N000141010139 P00003. I thank Juliane Schwendike for her translation of Prandtl (1932).

APPENDIX A

Revised Model Numerics

The original KW01 model used Marchuk operator-splitting for the time-stepping scheme (Marchuk 1974, chapter 4), in which the advection stage was followed by an adjustment stage (which modelled the Coriolis and pressure gradient terms), and then the physical processes. Operator-splitting schemes lose accuracy when processes that approximately balance are modelled in separate steps. In the tropical cyclone boundary layer, the centrifugal acceleration, which in a Cartesian-coordinate model is carried by the horizontal advection, is balanced to a large degree by the pressure gradient. Hence the time-stepping could be improved by moving all or part of the horizontal advection into the adjustment step.

The u-momentum equation for the model in a coordinate system moving at (u_{tc}, v_{tc}) is

$$\frac{\partial u}{\partial t}+(u-u_{tc})\frac{\partial u}{\partial x}+(v-v_{tc})\frac{\partial u}{\partial y}+w\frac{\partial u}{\partial z} = fv-\theta\frac{\partial \pi}{\partial x}+F_x \tag{A1}$$

where (u, v, w) is the earth-relative wind and F_x represents the friction terms. (This appendix uses Cartesian coordinates rather than the surface-layer coordinates used elsewhere.) Define an axisymmetric reference vortex $V = V(r)$ and associated Exner function Π in gradient balance with the local θ; only the gradients of Π are required and these are written in terms of V. Similarly π_{tc} is in geostrophic balance with (u_{tc}, v_{tc}). We then decompose

$$\pi = \Pi + \pi_{tc} + \pi^* \tag{A2}$$

$$u = -\frac{y}{r}V + u_{tc} + u^* \tag{A3}$$

$$v = \frac{x}{r}V + v_{tc} + v^* \tag{A4}$$

and the u-momentum equation becomes

$$\begin{aligned}\frac{\partial u^*}{\partial t} + (u-u_{tc})\frac{\partial u^*}{\partial x} + (v-v_{tc})\frac{\partial u^*}{\partial y} + w\frac{\partial u^*}{\partial z} = \\ \left\{-\frac{xy}{r^2}\left(\frac{V}{r}-\frac{\partial V}{\partial r}\right)u^*\right. \\ +\left[\frac{V}{r}-\frac{y^2}{r^2}\left(\frac{V}{r}-\frac{\partial V}{\partial r}\right)+f\right]v^* \\ \left.-\theta\frac{\partial \pi^*}{\partial x}\right\}+F_x.\end{aligned} \tag{A5}$$

Similarly, the v-momentum equation becomes

$$\begin{aligned}\frac{\partial v^*}{\partial t} + (u-u_{tc})\frac{\partial v^*}{\partial x} + (v-v_{tc})\frac{\partial v^*}{\partial y} + w\frac{\partial v^*}{\partial z} = \\ \left\{\frac{xy}{r^2}\left(\frac{V}{r}-\frac{\partial V}{\partial r}\right)v^*\right. \\ -\left[\frac{V}{r}-\frac{x^2}{r^2}\left(\frac{V}{r}-\frac{\partial V}{\partial r}\right)+f\right]u^* \\ \left.-\theta\frac{\partial \pi^*}{\partial y}\right\}+F_y.\end{aligned} \tag{A6}$$

These reduce to the original equations when the reference vortex $V = 0$. In the new numerics, the horizontal advection handles only the advection of (u^*, v^*) on the left-hand sides, while the adjustment step includes all the terms on the right-hand sides enclosed in curly brackets. Note that this decomposition is not a linearisation; all the nonlinear terms are retained. Rather, the purpose is to reduce the problem caused by the largely opposing tendencies from the horizontal advection and adjustment steps in the old scheme. As a further improvement, the code was upgraded from Marchuk to Strang operator splitting (Strang 1968; Gottlieb 1972).

The new code was compared to the old on a number of test cases, with various prescriptions of V including $V = 0$. The old code had the limitation that, with large timesteps, the opposing tendencies from the advection and adjustment steps could cause problems in the diagnosis of w using the continuity equation in the inner core. This limitation, which was previously avoided by using a small time step, is substantially alleviated by the new numerics. The choice of V is arbitrary, but in practice the obvious choice of using the same parametric tropical cyclone profile to (i) prescribe the upper boundary condition on π and (ii) for this decomposition is made.

APPENDIX B

The Relationship Between the Neutral Louis and Mellor-Yamada Schemes

We follow the notation of Mellor and Yamada (1982), particularly page 856, and further details may be found there. Simplify the level $2\frac{1}{4}$ scheme to the level 2 scheme by replacing the TKE budget equation with local production-dissipation balance,

$P_s + P_b = \epsilon$. Under neutral conditions the buoyant production $P_b = 0$. The shear production $P_s = KS^2$ with $K = lqS_M$, and the dissipation $\epsilon = q^3/(16.6l)$. Their eq. 41 and recommended values of the constants gives $S_M = 0.39$ for neutral conditions. Solving for q gives $q = 2.55lS$, whence $K = lqS_M = l^2S$, the neutral form of the Louis parameterisation.

REFERENCES

Andreas, E. L., 2004: Spray stress revisited. *J. Phys. Ocean.*, **34**, 1429–1440.

Black, P. G., et al., 2007: Air–sea exchange in hurricanes: Synthesis of observations from the coupled boundary layer air–sea transfer experiment. *Bull. Amer. Meteorol. Soc.*, **88**, 357–374.

Blackadar, A. K., 1962: The vertical distribution of wind and turbulent exchange in a neutral atmosphere. *J. Geophys. Res.*, **67**, 3095–3102.

Blackadar, A. K., 1976: Modelling the nocturnal boundary layer. *Preprints, 3rd Symposium on Atmospheric Turbulence Diffusion and Air Quality, Oct. 19-22, Raleigh, NC*, Amer. Meteorol. Soc., 46–49.

Blackadar, A. K., 1979: High-resolution models of the planetary boundary layer. *Advances in Environmental Science and Engineering*, J. R. Pfafflin and E. N. Ziegler, Eds., Gordon and Breach Sceince Publishers, New York, 50–85.

Braun, S. A. and W.-K. Tao, 2000: Sensitivity of high-resolution simulations of Hurricane Bob (1991) to planetary boundary layer parameterizations. *Mon. Wea. Rev.*, **128**, 3941–3961.

Bye, J. A. T. and A. D. Jenkins, 2006: Drag coefficient reduction at very high wind speeds. *J. Geophys. Res.*, **111**, doi:10.1029/2005JC003114.

Donelan, M. A., B. K. Haus, N. Reul, W. J. Plant, M. Stiassnie, H. C. Graber, O. B. Brown, and E. S. Saltzman, 2004: On the limiting aerodynamic roughness of the ocean in very strong winds. *Geophys. Res. Lett.*, **31**, L18 306, doi:10.1029/2004GL019460.

Drennan, W. M., J. Zhang, J. R. French, C. McCormick, and P. G. Black, 2007: Turbulent fluxes in the hurricane boundary layer. Part II: Latent heat flux. *J. Atmos. Sci.*, **64**, 1103–1115.

Eliassen, A., 1971: On the Ekman layer in a circular vortex. *J. Met. Soc. Japan*, **49**, 784–789.

Eliassen, A. and M. Lystad, 1977: The Ekman layer of a circular vortex. A numerical and theoretical study. *Geophysica Norvegica*, **7**, 1–16.

Foster, R. C., 2005: Why rolls are prevalent in the hurricane boundary layer. *J. Atmos Sci.*, **62**, 2647–2661.

Foster, R. C., 2009: Boundary layer similarity under an axisymmetric, gradient wind vortex. *Boundary-Layer Meteor.*, **131**, 321–344, doi:10.1007/s10546-009-9379-1.

Franklin, J. L., M. L. Black, and K. Valde, 2003: GPS dropwindsonde wind profiles in hurricanes and their operational implications. *Wea. Forecasting*, **18**, 32–44.

French, J. R., W. M. Drennan, J. A. Zhang, and P. G. Black, 2007: Turbulent fluxes in the hurricane boundary layer. Part I: Momentum flux. *J. Atmos. Sci.*, **64**, 1089–1102.

Gall, R., J. Tuttle, and P. Hildebrand, 1998: Small-scale spiral bands observed in Hurricanes Andrew, Hugo, and Erin. *Mon. Wea. Rev.*, **126**, 1749–1766.

Galperin, B., L. Kantha, S. Hassid, and A. Rosati, 1988: A quasi-equilibrium turbulent energy model for geophysical flows. *J. Atmos. Sci.*, **45**, 55–62.

Garratt, J. R., 1992: *The Atmospheric Boundary Layer*. Cambridge University Press, Cambridge, UK, 316 pp.

Gottlieb, D., 1972: Strang-type difference schemes for multidimensional problems. *SIAM J. Numer. Anal.*, **9**, 650–661.

Holland, G. J., 1980: An analytic model of the wind and pressue profiles in hurricanes. *Mon. Wea. Rev.*, **108**, 1212–1218.

Hong, S.-Y., Y. Noh, and J. Dudhia, 2006: New vertical diffusion package with an explicit treatment of entrainment processes. *Mon. Wea. Rev.*, **134**, 2318–2341.

Hong, S.-Y. and H.-L. Pan, 1996: Nonlocal boundary layer vertical diffusion in a medium-range forecast model. *Mon. Wea. Rev.*, **124**, 2322–2339.

Janjić, Z. I., 1994: The Step-Mountain Eta Coordinate Model: Further developments of the convection, viscous sublayer, and turbulence closure schemes. *Mon. Wea. Rev.*, **122**, 927–945.

Kalnay, E. and M. Kanamitsu, 1988: Time schemes for stronly nonlinear damping equations. *Mon. Wea. Rev.*, **116**, 1945–1958.

Katsaros, K. B., P. W. Vachon, W. T. Liu, and P. G. Black, 2002: Microwave remote sensing of tropical cyclones from space. *J. Oceanogr.*, **58**, 137–151.

Kepert, J. D., 2001: The dynamics of boundary layer jets within the tropical cyclone core. Part I: Linear theory. *J. Atmos. Sci.*, **58**, 2469–2484.

Kepert, J. D., 2006a: Observed boundary–layer wind structure and balance in the hurricane core. Part I: Hurricane Georges. *J. Atmos. Sci.*, **63**, 2169–2193, doi:10.1175/JAS3745.1.

Kepert, J. D., 2006b: Observed boundary–layer wind structure and balance in the hurricane core. Part II: Hurricane Mitch. *J. Atmos. Sci.*, **63**, 2194–2211, doi:10.1175/JAS3746.1.

Kepert, J. D., 2010a: Comparing slab and height-resolving models of the tropical cyclone boundary layer. Part I: Comparing the simulations. *Quart. J. Roy. Meteor. Soc.*, **136**, doi:10.1002/qj.667, 1689-1699.

Kepert, J. D., 2010b: Comparing slab and height-resolving models of the tropical cyclone boundary layer. Part II: Why the simulations differ. *Quart. J. Roy. Meteor. Soc.*, **136**, doi:10.1002/qj.685, 1700-1711.

Kepert, J. D., 2012: Choosing a boundary layer parameterisation for tropical cyclone modelling. *Mon. Wea. Rev.*, Early online release, doi:10.1175/MWR-D-11-00217.1.

Kepert, J. D. and Y. Wang, 2001: The dynamics of boundary layer jets within the tropical cyclone core. Part II: Nonlinear enhancement. *J. Atmos. Sci.*, **58**, 2485–2501.

Kimball, S. K. and F. C. Dougherty, 2006: The sensitivity of idealized hurricane structure and development to the distribution of vertical levels in MM5. *Mon. Wea. Rev.*, **134**, 1987–2008.

Langland, R. H. and C.-S. Liou, 1996: Implementation of an E-parameterization of vertical subgrid-scale mixing in a regional model. *Mon. Wea. Rev.*, **124**, 905–918.

Lock, A. P., A. R. Brown, M. R. Bush, G. M. Martin, and R. N. B. Smith, 2000: A new boundary layer mixing scheme. Part I: Scheme description and single-column model tests. *Mon. Wea. Rev.*, **128**, 3187–3199.

Lorsolo, S., J. L. Schroeder, P. Dodge, and F. D. Marks, Jr., 2008: An observational study of hurricane boundary layer small-scale coherent structures. *Mon. Wea. Rev.*, in press.

Lorsolo, S., J. A. Zhang, F. D. Marks, Jr., and J. Gamache, 2010: Estimation and mapping of hurricane turbulent energy using airborne Doppler measurements. *Mon. Wea. Rev.*, **138**, 3656–3670.

Louis, J. F., 1979: A parametric model of vertical eddy fluxes in the atmosphere. *Boundary-Layer Meteor.*, **17**, 187–202.

Louis, J. F., M. Tiedtke, and J. F. Geleyn, 1982: A short history of the operational PBL-parameterization at ECMWF. *Workshop on boundary layer parameterization, November 1981*, ECMWF, Reading, England, 59 – 79, URL `http://www.ecmwf.int/publications/library/ecpublications/_pdf/workshop/1981/PBL/ws_pbl_louis.pdf`.

Makin, V. K., 2005: A note on the drag of the sea surface at hurricane winds. *Boundary-Layer Meteor.*, **115**, 169176.

Marchuk, G. I., 1974: *Numerical Methods in Weather Prediction*. Academic Press, 277 pp., translated by K. N. Trirogoff and V. R. Lamb, Translation edited by A. Arakawa and Y. Mintz.

Mellor, G. L. and T. Yamada, 1982: Development of a turbulence closure model for geophysical fluid problems. *Rev. Geophys. and Space Phys.*, **20**, 851–875.

Moon, I.-J., I. Ginis, T. Hara, and B. Thomas, 2007: A physics-based parameterization of airsea momentum flux at high wind speeds and its impact on hurricane intensity predictions. *Mon. Wea. Rev.*, **135**, 2869–2878.

Moss, M. S., 1978: Low-level turbulence structure in the vicinity of a hurricane. *Mon. Wea. Rev.*, **106**, 841–849.

Moss, M. S. and F. J. Merceret, 1976: A note on several low-level features of Hurricane Eloise (1975). *Mon. Wea. Rev.*, **104**, 967–971.

Noh, Y., W. G. Cheon, S. Y. Hong, and S. Raasch, 2003: Improvement of the K-profile model for the planetary boundary layer based on large eddy simulation data. *Boundary-Layer Meteor.*, **107**, 401–427.

Nolan, D. S., 2005: Instabilities in hurricane-like boundary layers. *Dynamics of Atmospheres and Oceans*, **40**, 209–236.

Nolan, D. S., J. A. Zhang, and D. P. Stern, 2009a: Evaluation of planetary boundary layer parameterizations in tropical cyclones by comparison of in situ observations and high-resolution simulations of Hurricane Isabel (2003). Part I: Initialization, maximum winds, and the outer-core boundary layer. *Mon. Wea. Rev.*, **137**, 3651–3674.

Nolan, D. S., J. A. Zhang, and D. P. Stern, 2009b: Evaluation of planetary boundary layer parameterizations in tropical cyclones by comparison of in situ observations and high-resolution simulations of Hurricane Isabel (2003). Part II: Inner-core boundary layer and eyewall structure. *Mon. Wea. Rev.*, **137**, 3675–3698.

O'Brien, J. J., 1970: A note on the vertical structure of the eddy exchange coefficient in the planetary boundary layer. *J. Atmos. Sci.*, **27**, 1213–1215.

Powell, M. D., P. J. Vickery, and T. A. Reinhold, 2003: Reduced drag coefficient for high wind speeds in tropical cyclones. *Nature*, **422**, 279–283.

Prandtl, L., 1932: Meteorologische Anwendung der Strömungslehre. *Beitr. Physik der freien Atmosphäre, Bjerknes Festschrift*, **188**.

Rosenthal, S. L., 1962: A theoretical analysis of the field of motion in the hurricane boundary layer. National hurricane research project report no. 56, U. S. Department of Commerce, 12 pp.

Schwendike, J. and J. D. Kepert, 2008: The boundary–layer winds in Hurricanes Danielle (1998) and Isabel (2003). *Mon. Wea. Rev.*, **136**, 3168–3192.

Smith, R. K. and M. T. Montgomery, 2008: Balanced boundary layers used in hurricane models. *Quart. J. Roy. Meteor. Soc.*, **134**, 1385–1395.

Smith, R. K. and M. T. Montgomery, 2010: Hurricane boundary-layer theory. *Quart. J. Roy. Meteor. Soc.*, **136**, 1665–1670.

Smith, R. K., M. T. Montgomery, and V. S. Nguyen, 2009: Tropical cyclone spin-up revisited. *Quart. J. Roy. Meteor. Soc.*, **135**, 1321–1335.

Smith, R. K. and G. L. Thomsen, 2010: Dependence of tropical-cyclone intensification on the boundary-layer representation in a numerical model. *Quart. J. Roy. Meteor. Soc.*, **136**, 1671–1685.

Strang, G., 1968: On the construction and comparison of difference schemes. *SIAM J. Numer. Anal.*, **5**, 506–517.

Troen, I. and L. Mahrt, 1986: A simple model of the atmospheric boundary layer; sensitivity to surface evaporation. *Boundary-Layer Meteor.*, **37**, 129–148.

Wang, Y., 2007: A multiply nested, movable mesh, fully compressible, nonhydrostatic tropical cyclone model TCM4: Model description and development of asymmetries without explicit asymmetric forcing. *Meteorol. Atmos. Phys.*, **97**, 93–116.

Zhang, D. and R. A. Anthes, 1982: A high-resolution model of the planetary boundary layer—Sensitivity tests and comparisons with SESAME-79 data. *J. Appl. Met.*, **21**, 1594–1609.

Zhang, J. A., P. G. Black, J. R. French, and W. M. Drennan1, 2008a: First direct measurements of enthalpy flux in the hurricane boundary layer: The CBLAST results. *Geophys. Res. Lett.*, **35**, L14 813, doi:10.1029/2008GL034374.

Zhang, J. A., W. M. Drennan, P. G. Black, and J. R. French, 2009: Turbulence structure of the hurricane boundary layer between the outer rainbands. *J. Atmos. Sci.*, **66**, 2455–2467.

Zhang, J. A., K. B. Katsaros, P. G. Black, S. Lehner, J. R. French, and W. M. Drennan, 2008b: Effects of roll vortices on turbulent fluxes in the hurricane boundary layer. *Boundary-Layer Meteorol.*, **128**, 173–189.

Zhang, J. A., F. D. Marks, M. T. Montgomery, and S. Lorsolo, 2011a: An estimation of turbulent characteristics in the low-level region of intense Hurricanes Allen (1980) and Hugo (1989). *Mon. Wea. Rev.*, **139**, 1447–1462, doi:10.1175/2010MWR3435.1.

Zhang, J. A., R. F. Rogers, D. S. Nolan, and J. Marks, Frank D., 2011b: On the characteristic height scales of the hurricane boundary layer. *Mon. Wea. Rev.*, **139**, 2523–2535, doi:10.1175/MWR-D-10-05017.1.